

# Entropy and Bejan Number Influence on the Liquid Film Flow of Viscoelastic Hybrid Nanofluids in a Porous Space in Terms of Heat Transfer

Taza Gul, Safyan Mukhtar, Wajdi Alghamdi, Ishtiaq Ali, Anwar Saeed, and Poom Kumam\*



Cite This: *ACS Omega* 2022, 7, 33365–33374



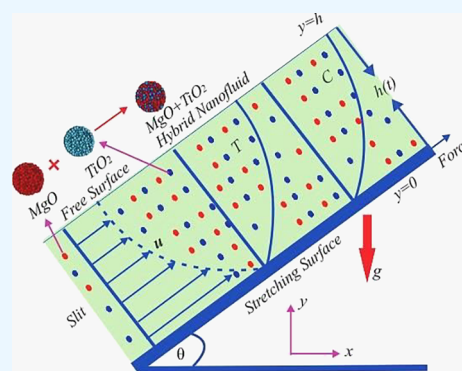
Read Online

ACCESS |

Metrics & More

Article Recommendations

**ABSTRACT:** The aim of this study is to determine the influence of the various parameters on the flow of thin film motion on an inclined extending surface. Maxwell fluid is used as a base fluid, and magnesium oxide (MgO) and titanium dioxide (TiO<sub>2</sub>) are used as nanocomponents. The width of the thin film is considered variable and varied according to the stability of the proposed model. The magnetic field is used in the vertical track to the flow field. The entropy generation and Bejan number are examined under the influence of various embedded parameters. The outputs of the liquid film motion, thermal profile, and concentration field are also shown with the help of their respective graphs based on the collected data. The solution of the model involves key features such as entropy generation, Bejan number, drag force, and heat transfer rate. Brinkman number, magnetic parameter, radiation parameter, thickness parameter  $\beta$ , and unsteadiness parameter  $S$  are also deliberated graphically. The percentage improvement for the enhancement of heat transfer has been calculated and compared for both the nanofluid and hybrid nanofluids. The results are validated through comparison with the existing literature.



## 1. INTRODUCTION

In nature, most of the existing fluids are not Newtonian, and it is not easy to study these fluids through simple Navier–Stokes equations without making alterations. Non-Newtonian fluids are needed in our daily lives, including food items, medications, polymers, and so on. These fluids are the combination of shear stresses and normal stresses. The time retardation effect, elasticity, and viscoelastic nature of these fluids make them different from the common fluids. These fluids have the tendency to improve the heat transfer rate efficiently and store energy due to their elastic nature. The researchers have also used these fluids for the cooling and thermal applications. The cooling and heating applications of these fluids are discussed by Hoyt<sup>1</sup> considering friction reduction. The other fruitful applications include pipelines carrying petroleum's which are made of high polymers in industries. Plastic materials are usually made of elastic fluids, and similarly, chemical and mining industries are dependent on Newtonian fluids. The viscoelastic fluids are more suitable for testing purposes in the form thin layers.

These tiny layers are widely used in the coating industry, including wire and fiber coatings. Thin films are usually used in lubrication to reduce the friction force and improve the device efficiency. Liquid films are more compatible to use for the heat transfer analysis. The basic ideas regarding thin film flow were investigated by Wang.<sup>2</sup> This idea is further improved by the

Andersson et al.<sup>3</sup> to add the energy equation. Similarly, new terminologies like the concept of pulse waves were used by researchers<sup>4,5</sup> in the flow regime of the thin film. In the initial studies, a constant thickness of the liquid film was used by the researchers, which was not so effective in maintaining the stability. Maintaining the stability of the thin film is more effective by using variable thickness instead of a constant thickness.<sup>6</sup> Thermal performance produces a dimensionless outcome that are restrained by an appliance that restores energy. The thickness of the thin film is very thin and quite suitable for heat transfer analysis in a short time at the laboratory level. Therefore, the researchers focus on the thin materials like the thin film for the testing purpose in terms of the heat transfer. Akkuş et al.<sup>7</sup> calculated liquid-film vapors considering 2D modeling. The thermal performance of the base liquids is commonly low, and nanoparticles or nanomaterials are usually stably dispersed in the base liquid to improve the thermal performance of the traditional fluid, known as nanofluids. Different mathematical models and various nano-

Received: June 27, 2022

Accepted: August 4, 2022

Published: September 8, 2022



materials were used by researchers<sup>8–22</sup> to improve the thermal performance of the base liquids. The efficiency in the heat transfer analysis can be seen in the mechanical, industrial, and renewable energy resources, and the proposed model is also a part of the enhancement in heat transfer considering hybrid nanofluids for the applications of renewable energy resources in terms of the theoretical analysis. Tahir et al.<sup>23</sup> have examined the behavior of various parameters using the liquid film flow.

The viscoelastic fluid flow in terms of thin film is commonly used in medication and industries. In fact, blood is a class of Maxwell fluid and some drugs also lie in the viscoelastic class of non-Newtonian fluids. Similarly, elastic materials are another form of the Maxwell fluid usually used in the industries. Maxwell fluid reveals both viscous and elastic performance, which means stress relaxation and elastic recovery after distortion are the main characteristics of the Maxwell fluid to distinguish this fluid from the rest of the non-Newtonian fluids. Nadeem et al.<sup>24</sup> have used the Maxwell fluid as a base fluid for thermal applications by inserting nanoparticles in the base solvent. They focused on the heat transfer rate and calculated all the thermal features related to the Maxwell fluid. Binetti et al.<sup>25</sup> have used the more reliable concepts by treating  $C_6H_9NaO_7$  in direct relation to the viscoelastic behavior of the Maxwell fluid. Sunnapwar and Pawar<sup>26</sup> used the same idea by using the stable thermophysical properties of the solid particles. Later on, the idea of using  $C_6H_9NaO_7$  for thermal performance has also been used.<sup>27,28</sup> These researchers correlated their studies with the agriculture sector.

Initially, working fluids with millimeter to micrometer sizes were used in renewable energy devices and the performance was not very encouraging. The use of working fluid containing an amalgamation of black liquid and micron-sized particles leads to erosion, sedimentation, and pipe blockage. Nanofluids are basically an amalgamation of nanosized nanofluid (<100 nanometers) metallic particles and the conventional liquid with extended heat transfer capabilities described by Bahiraei et al.<sup>29</sup>

The direct absorption of the nanofluids in the solar collector improved the thermal properties and is more effective in terms of the radiation characteristics as displayed in Al-Rashed et al.<sup>30</sup> The solution of the model is obtained by the researchers using the Keller box scheme.<sup>31–35</sup> The thermal performance of the nanofluids in the form of the direct absorption via solar collector using various nanoparticles, including silver and so on, was analyzed. The experiment depicted that a volume concentration of 3% with an ~10 mm collector height improves the efficiency by 90%. An analytical solution for the thermal radiation and the Joule heating impact for a thixotropic nanofluid flow is attained elsewhere.<sup>36</sup> A comparatively weaker boundary layer and low velocity of the fluid are witnessed for a strong magnetic field. Similar studies highlighting thermal radiation impacts on solar collectors are found elsewhere.<sup>37,38</sup> Free convection and thermic reaction convection were first introduced by Cess<sup>39</sup> and Arpaci.<sup>40</sup> Gul et al.<sup>41,42</sup> analyzed nanofluid flow using various models for the applications of heat transfer. Takabi & Salehi<sup>51</sup> analyzed hybrid nanofluids using the mathematical model of the sinusoidal enclosures for thermal applications. Hybrid nanofluid is the combination of the stable dispersion of different nanoparticles having different thermophysical and chemical properties in the same base fluid. These are widely used in the heat exchangers, solar systems, and drug deliveries.<sup>43–50</sup>

The Maxwell fluid thin film flow over an extending surface has been examined by Takabi and Salehi.<sup>51</sup> The idea regarding heat and mass transfer including the variable thickness of the liquid film was discussed by Qasim et al.<sup>52</sup> The concept of  $TiO_2$  and Ag materials for the drug delivery was analyzed by Charegh and Dinarvand<sup>53</sup> using blood as the base fluid. Gul and Pervez<sup>54</sup> have used the thin film of Maxwell hybrid nanofluids for various thermal applications. They observed the thermophoresis' and Brownian motion parameters' impact on the liquid film flow. The viscoelastic fluids were used by researchers<sup>55,56</sup> for heat transfer enhancement applications. The thermal effect is mostly targeted by researchers to improve energy resource efficiency.

Originality/Value

- The entropy generation in the liquid film using Maxwell fluid is a new addition.
- The Bejan number impact under the influence of various parameters improves the novelty of the suggested model.
- $MgO$  and  $TiO_2$  nanomaterial dispersion in the Maxwell fluid to perform hybrid nanofluids for the enhancement of heat transformation is a very rare approach in the form of thin film.
- The thin film Maxwell hybrid nanofluids in terms of the  $MgO$  and  $TiO_2$  nanomaterials are a new extension for the heat and mass transfer analysis.
- A porous medium, thermal radiation, and magnetic parameters further improve the novelty of the thin film fluid flow on an inclined plane.

**1.1. Methodology.** The proposed flow model was developed through a system of PDEs, which later is transformed into non-linear ODEs. The homotopy analytical method (HAM) in MATHEMATICA has been used for the analytical solution of the proposed model.

## 2. FORMATION

In the proposed flow demonstration, we took into account the thin-layer flow of the Maxwell hybrid nanofluid on an inclined extending surface, and the Maxwell fluid has been used as a base fluid. Two  $MgO$  and  $TiO_2$  nanomaterials are used in hybrid nanofluid preparation.

As the fluid lies on the extending sheet as force is applied to the sheets, they start moving.  $h(t)$  represents the thickness of the film.

In the above figure, the extending sheet is placed inclined to make an angle  $\phi$  with the horizontal plane. When we apply force on the sheet, it starts moving with a velocity

$$U = bx(1 - at)^{-0.5} \quad (1)$$

The operative elasticity of the velocity is  $b(1 - at)^{-1/2}$  toward the  $x$  axis, and the parameter " $a$ " stands for the increment of time in a selected range ( $0 \leq a < 1$ ) while " $b$ " represents the elasticity. The surface temperature of the extending sheet is signified as " $T_s$ ", and the temperatures of the slit are defined as  $T_0$  and  $T_r$ . The range of these constraints are referred to as  $0 \leq T_r \leq T_0$ .

The unsteady magnetic term in a perpendicular track is defined as

$$B_0(x, t) = (1 - at)^{-1/2} B_0 \quad (2)$$

The basic flow equations are

$$\frac{\partial u}{\partial x} + \frac{\partial v}{\partial y} = 0 \quad (3)$$

$$\begin{aligned} & \left( \frac{\partial u}{\partial t} + u \frac{\partial u}{\partial x} + v \frac{\partial u}{\partial y} \right) \\ &= v_{hmf} \frac{\partial^2 u}{\partial y^2} - \lambda_1 \left( 2uv \frac{\partial^2 u}{\partial x \partial y} + u^2 \frac{\partial^2 u}{\partial x^2} + v^2 \frac{\partial^2 u}{\partial y^2} \right) \\ & - \frac{v_{hmf}}{k^\oplus} \left( \lambda_1 v \frac{\partial u}{\partial y} + u \right) + g \{ \pm (T - T_h) (\beta_T)_{hmf} \\ & + (C - C_h) (\beta_C)_{hmf} \} \sin \theta \end{aligned} \quad (4)$$

$$\frac{\partial T}{\partial t} + u \frac{\partial T}{\partial x} + v \frac{\partial T}{\partial y} = \alpha_{hmf} \left[ \frac{\partial^2 T}{\partial y^2} \right] + \frac{16\sigma^* T_h^3}{3k^*(\rho C_p)_{hmf}} \frac{\partial^2 T}{\partial y^2} \quad (5)$$

$$\frac{\partial C}{\partial t} + u \frac{\partial C}{\partial x} + v \frac{\partial C}{\partial y} = D_{Bhmf} \frac{\partial^2 C}{\partial y^2} - Kr(C - C_h) \quad (6)$$

The components of velocity are represented by  $u$ ,  $v$ , which are acting along the directions of  $x$  and  $y$ , respectively. The physical conditions for the thin film flow is defined as

$$\begin{aligned} u|_{y=0} = U_w, \quad v|_{y=0} = 0, \quad \mu_{hmf} \frac{\partial u}{\partial y} \Big|_{y=h(t)}, \quad v = \frac{\partial h}{\partial t} \Big|_{y=h(t)}, \\ T|_{y=0} = T_w, \quad C|_{y=0} = C_w, \quad \frac{\partial T}{\partial y} \Big|_{y=h(t)} = \frac{\partial C}{\partial y} \Big|_{y=h(t)} = 0 \end{aligned} \quad (7)$$

$h(t)$  stands for the liquid film width.

$$\begin{aligned} \psi &= \left( \frac{bv}{1-\alpha t} \right)^{1/2} x f(\eta), \quad u = \frac{\partial \psi}{\partial y}, \quad v = -\frac{\partial \psi}{\partial x}, \\ \eta &= \left( \frac{b}{v(1-\alpha t)} \right)^{1/2} y, \quad T = T_0 - T_r \left( \frac{bx^2}{2v} \right) \frac{\Theta(\eta)}{(1-\alpha t)^{3/2}}, \\ C &= C_0 - C_r \left( \frac{bx^2}{2v} \right) \frac{\Phi(\eta)}{(1-\alpha t)^{3/2}} \end{aligned} \quad (8)$$

The transformed form is displayed as follows:

$$\beta = \left( \frac{b}{v(1-\alpha t)} \right)^{1/2} h(t) \quad (9)$$

$$\frac{dh}{dt} = \frac{\alpha\beta}{2} \left( \frac{v}{b(1-\alpha t)} \right)^{1/2} \quad (10)$$

$$\begin{aligned} & \frac{\mu_{hmf}}{\mu_f} \frac{\rho_f}{\rho_{hmf}} f''' - (f')^2 + ff'' + \lambda(2ff'f'' - f^2 f''') \\ & - S \left( f' + \frac{\eta}{2} f'' \right) - \lambda r (f' - \lambda ff'') \pm \frac{\beta_{Thmf}}{\beta_f} (Gr\Theta) \\ & + \frac{\beta_{Chmf}}{\beta_f} (Gc\Phi) \\ & = 0 \end{aligned} \quad (11)$$

$$\begin{aligned} & \frac{1}{Pr} \frac{(\rho C_p)_f}{(\rho C_p)_{hmf}} \left( \frac{k_{hmf}}{k_f} + \frac{4}{3} Rd \right) \Theta'' - \frac{S}{2} (3\Theta + \eta\Theta') - 2f'\Theta \\ & + f\Theta' = 0 \end{aligned} \quad (12)$$

$$\Phi'' + Sc \left( \frac{S}{2} (3\Phi + \eta\Phi') - 2f'\Phi + f\Phi' \right) - \gamma Sc\Phi = 0 \quad (13)$$

$$\begin{aligned} S &= \frac{\alpha}{a}, \quad \lambda = \frac{\lambda_1}{(1-\alpha t)}, \quad \lambda r = \frac{v}{k^\oplus a}, \quad Pr = \frac{\mu C_p}{k}, \\ Rd &= \frac{4\sigma^* T_h^3}{3k^* k_f (\rho C_p)_{hmf}}, \quad \gamma = \frac{Kr}{a}, \quad Gr = \frac{g\beta_{Tf} [T_w - T_h] x^3}{v_f^2}, \\ Gc &= \frac{g\beta_C [C_w - C_h] x^3}{v_f^2} \end{aligned} \quad (14)$$

where  $S$ ,  $\lambda r$ ,  $Pr$ ,  $\lambda$ ,  $\gamma$ ,  $Gr$ ,  $Rd$ , and  $Gc$  are the unsteadiness parameter, porosity term, Prandtl number, Maxwell parameter, chemical reaction, thermal Grashof number, radiation parameter, and mass Grashof number, respectively.

The transformed form of the physical conditions are taken as

$$\begin{aligned} f(0) = 0, \quad f'(0) = 1, \quad \Theta(0) = 1, \quad \Phi(0) = 1 \\ f''(\beta) = 0, \quad f(\beta) = \frac{S\beta}{2}, \quad \Theta'(\beta) = 0, \quad \Phi'(\beta) = 0 \end{aligned} \quad (15)$$

$$C_f = \frac{2\tau_w}{\rho U_w^2}, \quad N_u = \frac{q_w x}{k(T_w - T_0)}, \quad S_n = \frac{q_m x}{D_B(C_w - C_0)} \quad (16)$$

$$\tau_w = \mu \left( \frac{\partial u}{\partial y} \right) \Big|_{y=0}, \quad q_w = -k \left( \frac{\partial T}{\partial y} \right) \Big|_{y=0}, \quad q_m = -D_B \left( \frac{\partial C}{\partial y} \right) \Big|_{y=0}$$

These terms are transformed and in the simplified form are displayed as

$$\begin{aligned} Re^{1/2} C_f &= -\frac{\mu_f}{\mu_{hmf}} f''(0), \quad Re^{-1/2} Nu = -\left( \frac{k_{hmf}}{k_f} + Rd \right) \Theta'(0), \\ Re^{-1/2} S_h &= -\Phi'(0), \quad Re = \frac{x U_w}{\nu} \end{aligned} \quad (17)$$

**2.1. Entropy Rate.** Entropy is an essential idea in engineering, mathematical models, and physics. It plays a vital role in continuum physics, thermodynamics, biology, and economics.<sup>57–60</sup> Entropy is actually a phenomenon dependent on the second law of thermodynamics, which states that entropy increases in an isolated system through any activity. While this idea is further extended in quantum mechanics with the inclusion of a density matrix. In the case of the statistical system or in the theory of probability, entropy is used to measure the uncertainty of the variables that are used in the statistical phenomena.

$$S_g = \frac{1}{T_\infty^2} \left( k_{hmf} + \frac{16\sigma^* T_h^3}{3k^*} \right) \left( \frac{\partial T}{\partial y} \right)^2 + \frac{\mu_{hmf}}{T_\infty} \left( \frac{\partial u}{\partial y} \right)^2 + \frac{\mu_{hmf}}{T_\infty K} (u)^2 + \frac{RD}{C_\infty} \left( \frac{\partial C}{\partial y} \right)^2 + \frac{RD}{T_\infty} \frac{\partial C}{\partial y} \frac{\partial T}{\partial y}$$

$$S_G = \left( \frac{k_{hmf}}{k_f} + Rd \right) \lambda (\Theta')^2 + PrEc [(1 - \phi_1)^{-2.5} (1 - \phi_2)^{-2.5} (f'')^2 + \lambda r (f')^2 + L(\Theta'\Phi' + (\Phi')^2)] \tag{18}$$

Here,  $S_G = \frac{S_g T_\infty}{(T_w - T_\infty)}$  is the rate of entropy generation,  $L = \frac{RD(C_w - C_\infty)}{k_f}$  is the diffusive parameter, and  $\lambda = \frac{T_w - T_\infty}{T_\infty}$  is the temperature difference parameter.

**2.2. Bejan Number.** The irreversibility due to heat transfer ratio to total irreversibility is called the Bejan number.

$$Be = \left[ \frac{k_{hmf}}{k_f} \lambda (\Theta')^2 \right] / \left[ \left( \frac{k_{hmf}}{k_f} + Rd \right) \lambda (\Theta')^2 + PrEc [(1 - \phi_1)^{-2.5} (1 - \phi_2)^{-2.5} (f'')^2 + \lambda r (f')^2 + L(\Theta'\Phi' + (\Phi')^2)] \right] \tag{19}$$

### 3. RESULTS AND DISCUSSION

The viscoelastic influence can significantly worsen the critical Reynolds number of comparable shear flows. The Oldroyd B

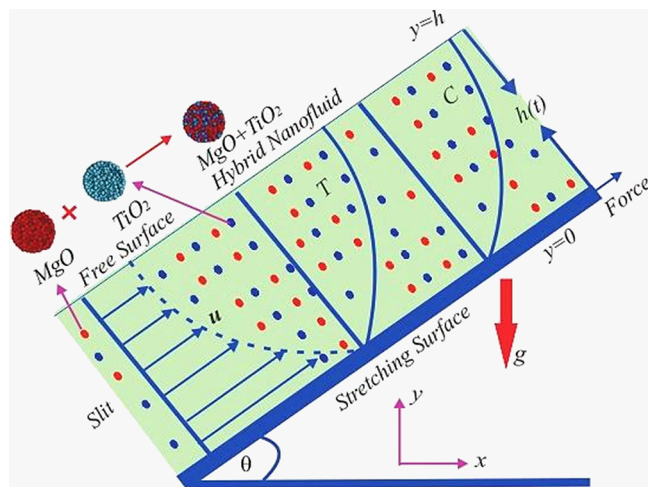


Figure 1. Physical sketch of the proposed model.

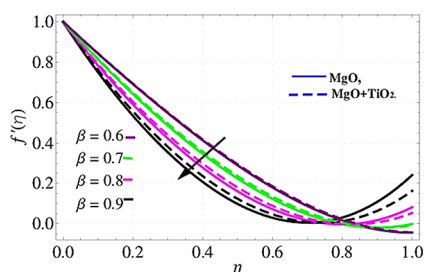


Figure 2. Consequence of  $\beta$  vs  $f'(\eta)$ .

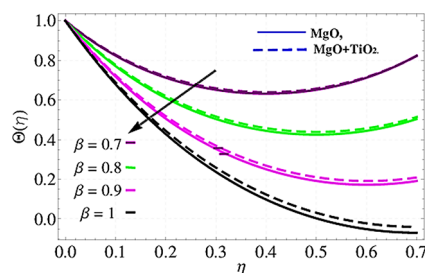


Figure 3. Consequence of  $\beta$  vs  $\Theta(\eta)$ .

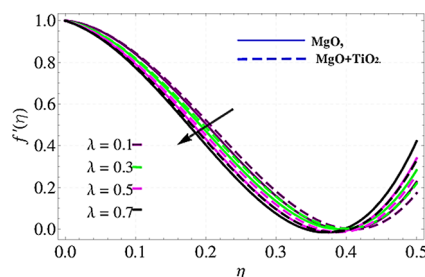


Figure 4. Consequence of  $\lambda$  vs  $f'(\eta)$ .

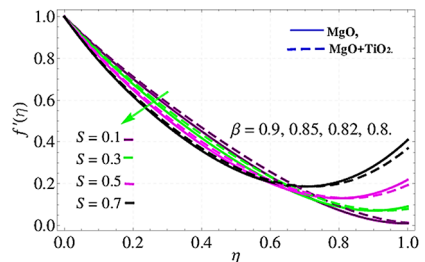


Figure 5. Consequence of  $S$  vs  $f'(\eta)$ .

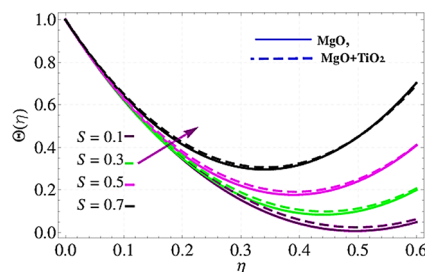


Figure 6. Consequence of  $S$  vs  $\Theta(\eta)$ .

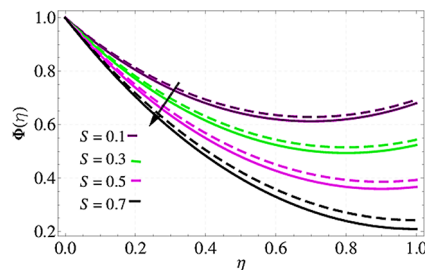
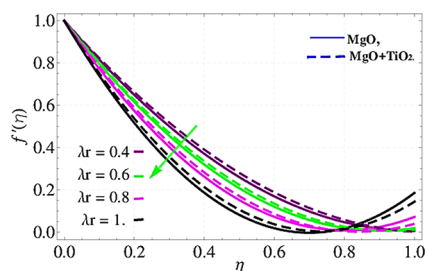
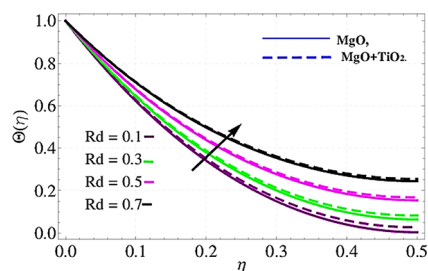
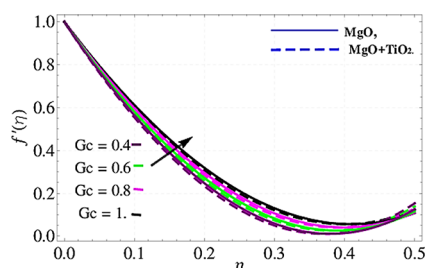
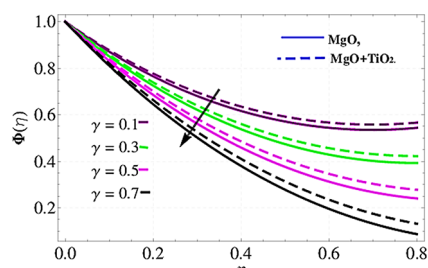
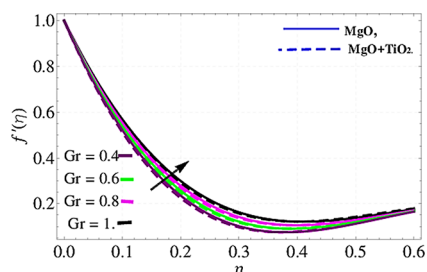
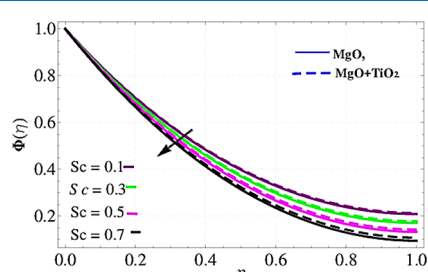
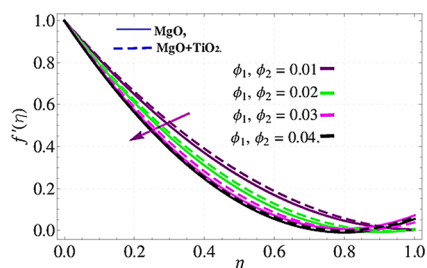
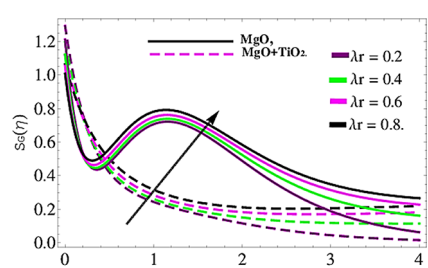
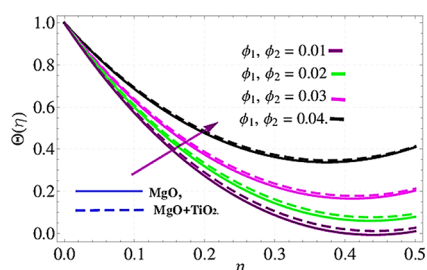
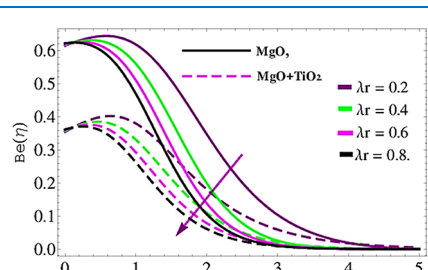


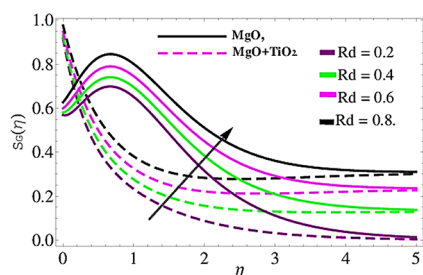
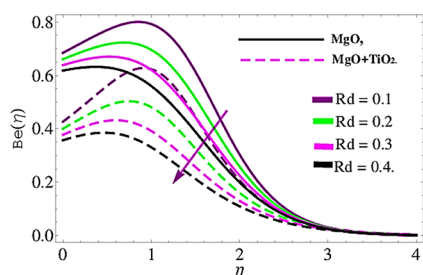
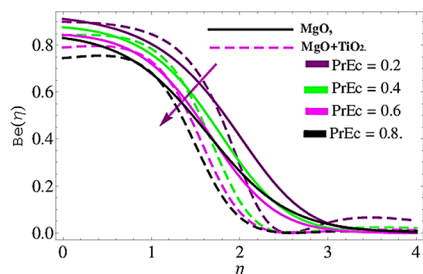
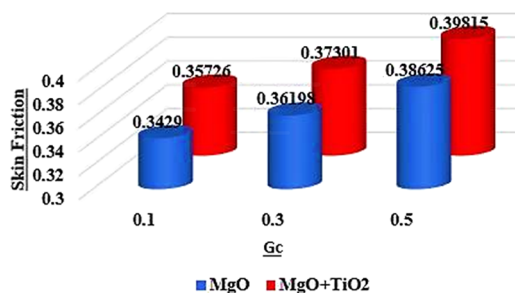
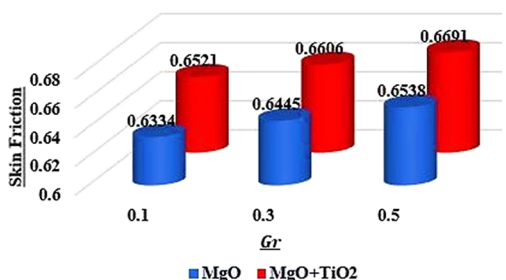
Figure 7. Consequence of  $S$  vs  $\Phi(\eta)$ .

and Maxwell fluids are the most systematically studied. The critical Reynolds number is more visible in the tiny layers like thin liquid films. The flow of Maxwell hybrids on an inclined and stretching sheet is taken into consideration.

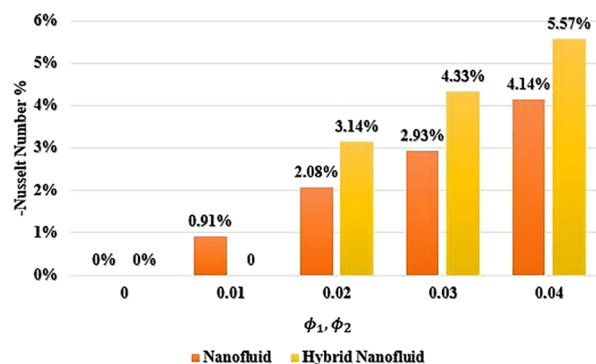
Figure 8. Consequence of  $\lambda r$  vs  $f'(\eta)$ .Figure 13. Consequence of  $Rd$  vs  $\Theta(\eta)$ .Figure 9. Consequence of  $Gc$  vs  $f'(\eta)$ .Figure 14. Consequence of  $\gamma$  vs  $\Phi(\eta)$ .Figure 10. Consequence of  $Gr$  vs  $f'(\eta)$ .Figure 15. Consequence of  $Sc$  vs  $\Phi(\eta)$ .Figure 11. Consequence of  $\phi_1, \phi_2$  vs  $f'(\eta)$ .Figure 16. Consequence of  $\lambda r$  vs  $NG$ .Figure 12. Consequence of  $\phi_1, \phi_2$  vs  $\Theta(\eta)$ .Figure 17. Consequence of  $\lambda r$  vs  $Be$ .

Solid nanoparticles (NPs) from magnesium oxide (MgO) and titanium dioxide ( $\text{TiO}_2$ ) are used to produce hybrid nanofluids. These nanoparticles are dispersed in the Maxwell fluid efficiently up to 5% of the total fluid. The mathematical model in the form of nonlinear ODEs has been applied using a

well-known seminumerical technique (HAM). The latest version or package BVPh 2.0 of this method is a more reliable version to sustain the stability, and convergence is used here to find out the solution. The key objective of this study is to

Figure 18. Consequence of  $Rd$  vs  $NG$ .Figure 19. Consequence of  $Rd$  vs  $Be$ .Figure 20. Consequence of  $Br = EcPr$  vs  $Be$ .Figure 21. Consequence of  $Gc$  vs skin friction.Figure 22. Consequence of  $Gr$  vs skin friction.

investigate the heat transfer rate enhancement using the hybrid nanofluid, and it is observed that hybrid nanofluids are more

Figure 23. Consequence of  $\phi_1, \phi_2$  vs Nusselt number enhancement in %.

reliable to improve the heat transfer rate. The physical structure of the problem is revealed in Figure 1.

Figures 2 and 3 show the consequence under  $\beta$ . As  $\beta$  upsurges, the velocity field declines, but the temperature field rises due to the increased film thickness.

The film width causes the enhancement in the distribution of velocity components in the downward direction. Physically, the increasing thickness of the liquid film progresses the resistance force and consequently the fluid motion decline. It is also noted that hybrid nanofluids ( $TiO_2 + MgO$ ) are more effective than nanofluids ( $MgO$ ) used for  $\beta$  variation.

The axwell parameter influence is displayed in Figure 4.

The fluid movement changes in relation to the Maxwell parameter  $\lambda$ . Therefore, the change of  $\lambda$  disrupts the velocity profile. Thus, the increase of  $\lambda$  decreases the movement of the liquid film. The viscoelasticity parameter increment increases the resistive force and as a result the fluid flow decline.

Figures 5–7 illustrates the impact of " $S$ " in the suggested model; it was noted that the parameter " $S$ " has a significant impact on  $f'(\eta)$  and  $\Theta(\eta)$ .

The intensification in " $S$ " explains a decrease in the velocity field; likewise, an increase in the temperature distribution is caused by an upsurge in " $S$ ". Liquid film motion was expressively decreased due to the increasing values of the instability parameter.

These outputs depict the nature of the unstable parameter resulting in a drop in the liquid film thickness  $\beta$ . The distinction in the liquid film thickness bears the stability of the fluid motion, and also the convergence is mainly based on the thickness of the liquid film. Also, the concentration profile decreases with the higher values of  $S$ . Figure 8 illustrates the behavior of the porosity parameter " $\lambda r$ ". It is seen that for increasing the porous parameter, the velocity declines. The declining trend is due to the fact that the increased porous parameter dominates the frictional effects.  $MgO$  and  $TiO_2 + MgO$  nanomaterials are melted in the Maxwell liquid to perform nanofluid and hybrid nanofluids. The resistance force is initiated due to the larger liquid film thickness  $\beta$ , and the same influence is produced with the rising value of the porosity parameter " $\lambda r$ ". Therefore, the resistance force is improved with the increasing value of the porosity parameter.

Figures 9 and 10 display the influence of the  $Gc$  (Mass Grashof number) over the liquid film motion. The mass Grashof number is acting along the flow direction, and therefore the augmentation of  $Gc$  enhances the fluid motion. The increasing effect is further improved in terms of the hybrid nanofluids.

**Table 1. Thermophysical Features of the Nanoparticles**

parameter	APS (average particle size), nm	mMorphology	true density, g cm <sup>-3</sup>	thermal conductivity, W m <sup>-1</sup> k <sup>-1</sup>	specific heat capacity, J kg <sup>-1</sup> K <sup>-1</sup>
MgO	25–45	nearly spherical	3.57	5.112	0.852
TiO <sub>2</sub>	18–23	nearly spherical	3.95	5.407	0.835
80 wt % MgO-20 wt % TiO <sub>2</sub>	10–45	spherical	2.87	4.768	0.842

**Table 2. Comparison between the Published Work and Present Work for the Surface and Wall Temperature Gradients Considering Common Factors Using the Regular Fluid Having  $Pr = 7.56^a$** 

	Wang <sup>2</sup>	Wang <sup>2</sup>	Qasim et al. <sup>52</sup>	Qasim et al. <sup>52</sup>	present	present
S	$\Theta(1)$	$-\Theta'(0)$	$\Theta(\beta)$	$-\beta\Theta'(0)$	$\Theta(\beta)$	$-\beta\Theta'(0)$
0.1	0.34201	0.5302	0.34810	0.53263	0.348320	0.532865
3	0.65321	1.20437	0.67224	1.31026	0.681210	1.34720
6	1.02531	1.72810	1.05168	1.81321	1.062102	1.85210
9	1.73106	2.23017	1.82021	2.37630	1.881312	2.413021

<sup>a</sup>Note that they used small and variables values of the Prandtl number.

**Table 3. Comparison between the Published Work and Present Work for the Sherwood Number Considering a Common Factor Using the Regular Fluid Having  $Pr = 7.56$ ,  $S = 10$** 

	Qasim et al. <sup>52</sup>	Qasim et al. <sup>52</sup>	present	present
$Sc$	$\Phi(\beta)$	$-\Phi'(0)$	$\Phi(\beta)$	$-\Phi'(0)$
10	0.31264	0.72018	0.31301	0.723510
12	0.21235	0.68382	0.21423	0.69310
14	0.13641	0.52103	0.13910	0.55102

The increasing values of the thermal Grashof number in terms of linear temperature difference enhance the fluid motion and this effect is more effective by using hybrid nanofluids (MgO and TiO<sub>2</sub>).

Figures 11 and 12 show the nanoparticle volume fraction ( $\phi_1$ ,  $\phi_2$ ) for velocity and thermal profiles. The increasing values of the nanoparticle volume fraction in a particular range ( $\phi_1$ ,  $\phi_2 = 0.01, 0.02, 0.03$ ) reduce the velocity field and boost the temperature distribution.

The obtained outputs show that those hybrid nanofluids containing MgO + TiO<sub>2</sub> nanomaterial progress the thermal characteristics of the conventional fluids. The target of the proposed model is to progress the thermal transport of the conventional fluids, and the addition of the radiation term shown in Figure 13 improves the temperature distribution. Again, the increasing amount of  $Rd$  boosts the temperature profile.

Increasing values of chemical reaction  $\gamma$  reduce the concentration field as shown in Figure 14. The cohesive forces between the molecules increase due to the increasing values of the chemical reactions, which reduces the concentration field. The augmentation in the Schmidt number ( $Sc$ ) also reduces the concentration profile, and this happens due to the reduction in the molecular diffusion as shown in Figure 15.

The entropy regime enhances with the cumulative values of the porosity parameter while the opposite trend is achieved in the case of the Bejan number as shown in Figures 16 and 17. Similarly, the thermal growth upsurges with the accumulation in the radiation parameter, and thus the entropy of the fluid upsurges while the Bejan number decreases as shown in Figures 18 and 19.

A plot of the Bejan number versus Brinkman number is displayed in Figure 20. The Bejan number declines with the augmentation in the Brinkman number. In fact, fluid and

entropy upsurge with an increase in the Brinkman number, and the Bejan number plays a reverse role of entropy.

The statistical analysis was also done for the imperative parameters like skin friction (drag force), Nusselt number (heat transfer rate), and Sherwood number. The comparative analysis for the nanofluid and hybrid nanofluid has been performed in terms of the above physical parameters. The increment in the mass Grashof number  $Gc$  improves the liquid film flow, as displayed in Figure 21. Physically, the ways of the flow and mass Grashof number are in the same direction and the increasing value of the mass Grashof number improves the fluid velocity, and therefore the skin friction declines.

The thermal Grashof number influence on the skin friction is displayed in Figure 22. Again, the greater values of the  $Gr$  improve the liquid film flow and decline the skin friction. Figure 23 shows the consequences of  $\phi_1$ ,  $\phi_2$ . The thermal profile and thermal transport rate are more enhanced due to the increasing amount of the nanoparticle volume fraction. The hybrid nanofluid is more effective in comparison with nanofluids and conventional fluids to enhance the heat transfer rate as shown in Figure 23. The percentage-wise enhancement in the heat transfer provides more evidence to show that hybrid nanofluids have the tendency to improve the heat transfer rate more efficiently. The thermophysical properties of the solid nanoparticles are displayed in Table 1. The comparisons of the proposed model with the published work are shown in Tables 2 and 3. The Prandtl number values remain fixed in all the existing and current work. As per the experimental approach, the Prandtl number is fixed and does not vary for the regular fluid. Therefore, the common parameter, the unsteadiness  $S$ , was compared with the published work,<sup>2,52</sup> and as a result a much closer agreement was attained. As Wang's<sup>2</sup> study is limited up to heat transfer, the variation in the Schmitt number, which is a common parameter of the concentration profile among the present work and that of Qasim et al.,<sup>52</sup> has been compared for the various values. The comparison shows the authentication of the present results with the existing literature.

#### 4. CONCLUSIONS

The current study delineates the effect of nanocomposites on the Maxwell hybrid nanofluid. The heat transfer rate for various parameters in the presence of radiation, magnetic field, and porosity is analyzed in the form of physical and

computational data. Mass transfer and entropy factors are considered in this model.

The problem is tackled through the homotropy analysis method (HAM) in MATHEMATICA. The proposed flow model is very worthwhile and valuable in various physical processes involving heat and mass phenomena. This work demonstrated its productivity and valuable usage in medical sciences, engineering, and other industries.

The key conclusions are the following:

- The growing inputs of the thermal Grashof number increase the fluid motion.
- The thermal field grows with the augmentation in the volume fraction of the nanoparticles, and this effect is more effective in terms of the hybrid nanofluids.
- Increasing the width of the film would cause the velocity profile to increase.
- The large value of the magnetic moment parameter would cause the Lorentz force enhancement, and therefore the deceleration in fluid motion occurs.
- The percentage-wise improvement in the heat transfer rate confirms that the hybrid nanofluids are more effective at enhancing heat transfer.
- The entropy of the hybrid nanofluids increases with increasing porosity parameter, and for the same variation of the porosity parameter, the Bejan number decreases.
- The radiation parameter increases the entropy of the hybrid nanofluids for its larger values and reduces the Bejan number.

## AUTHOR INFORMATION

### Corresponding Author

**Poom Kumam** – Center of Excellence in Theoretical and Computational Science (TaCS-CoE), Faculty of Science, King Mongkut's University of Technology Thonburi (KMUTT), Bangkok 10140, Thailand; Department of Medical Research, China Medical University Hospital, China Medical University, Taichung 40402, Taiwan; Email: [poom.kum@kmutt.ac.th](mailto:poom.kum@kmutt.ac.th)

### Authors

**Taza Gul** – Department of Mathematics, City University of Science and Information Technology, Peshawar 25000, Pakistan; [orcid.org/0000-0003-1376-8345](https://orcid.org/0000-0003-1376-8345)

**Safyan Mukhtar** – Department of Basic Sciences, Preparatory Year Deanship King Faisal University, Al-Ahsa 31982, Saudi Arabia

**Wajdi Alghamdi** – Department of Information Technology, Faculty of Computing and Information Technology, King Abdulaziz University, Jeddah 80261, Saudi Arabia

**Ishtiaq Ali** – Department of Mathematics and Statistics, College of Science, King Faisal University, 31982 Al-Ahsa, Saudi Arabia

**Anwar Saeed** – Center of Excellence in Theoretical and Computational Science (TaCS-CoE), Faculty of Science, King Mongkut's University of Technology Thonburi (KMUTT), Bangkok 10140, Thailand; [orcid.org/0000-0003-1566-6457](https://orcid.org/0000-0003-1566-6457)

Complete contact information is available at:  
<https://pubs.acs.org/10.1021/acsomega.2c03975>

## Author Contributions

Data curation, T.G., S.M., W.A.; conceptualization, T.G.; formal analysis, T.G., S.M., W.A.; methodology, T.G., S.M., W.A.; project administration, A.S., P.K., I.A.; Entropy and Bejan number validation, A.S., P.K., I.A.

## Notes

The authors declare no competing financial interest.

## ACKNOWLEDGMENTS

The authors acknowledge the financial support provided by the Center of Excellence in Theoretical and Computational Science (TaCS-CoE), KMUTT. Moreover, this research project is supported by Thailand Science Research and Innovation (TSRI) Basic Research Fund: Fiscal year 2022 under project number FRB650048/0164.

## NOMENCLATURE

$\lambda_1$	time relaxation
$\tau$	extra stress tensor
$\kappa$	thermal conductivity
$C_p$	specific heat
$Pr$	Prandtl number
$T_0, T_{ref}$	constant temperature
$S$	unsteadiness parameter
$T$	temperature
$\nu_{hnf}$	kinematic viscosity of hybrid nanofluid
$u, v$	velocity components
$\rho$	density
$\mu_{hnf}$	dynamic viscosity of hybrid nanofluid
$Sc$	Schmitt number
$k^\oplus$	permeability coefficient
$\lambda$	time relaxation
$\eta$	similarity variable
$\Theta$	temperature in non-dimensional form
$h(t)$	thickness of the film

## REFERENCES

- (1) Hoyt, J. W. Some applications of non-Newtonian fluid flow. In *Rheology Series*; Elsevier, 1999; pp. 797–826, DOI: [10.1016/S0169-3107\(99\)80008-2](https://doi.org/10.1016/S0169-3107(99)80008-2).
- (2) Wang, C. Y. Liquid film on an unsteady stretching surface. *Q. Appl. Math.* **1990**, *48*, 601–610.
- (3) Andersson, H. I.; Bech, K. H.; Dandapat, B. S. Magneto-hydrodynamic flow of a power-law fluid over a stretching sheet. *Int. J. Non-Linear Mech.* **1992**, *27*, 929–936.
- (4) Dandapat, B. S.; Singh, S. K.; Maity, S. Thin film flow of bi-viscosity liquid over an unsteady stretching sheet: an analytical solution. *Int. J. Mech. Sci.* **2017**, *130*, 367–374.
- (5) Adebayo, I.; Xie, Z.; Che, Z.; Matar, O. K. Doubly excited pulse waves on thin liquid films flowing down an inclined plane: An experimental and numerical study. *Phys. Rev. E* **2017**, *96*, No. 013118.
- (6) Gul, T.; Khan, M. A.; Khan, A.; Shuaib, M. Fractional-order three-dimensional thin-film nanofluid flow on an inclined rotating disk. *Eur. Phys. J. Plus* **2018**, *133*, 500.
- (7) Akkuş, Y.; Tarman, H. I.; Çetin, B.; Dursunkaya, Z. Two-dimensional computational modeling of thin film evaporation. *Int. J. Therm. Sci.* **2017**, *121*, 237–248.
- (8) Sarlak, R.; Yousefzadeh, S.; Akbari, O. A.; Toghraie, D.; Sarlak, S.; assadi, F. The investigation of simultaneous heat transfer of water/Al<sub>2</sub>O<sub>3</sub> nanofluid in a close enclosure by applying homogeneous magnetic field. *Int. J. Mech. Sci.* **2017**, *133*, 674–688.
- (9) Esfe, M. H.; Akbari, M.; Toghraie, D. S.; Karimipour, A.; Afrand, M. Effect of nanofluid variable properties on mixed convection flow and heat transfer in an inclined two-sided lid-driven cavity with

sinusoidal heating on sidewalls. *Heat Transfer Res.* **2014**, *45* (), DOI: 10.1615/HeatTransRes.2013007127.

(10) Li, Z.; Barnoon, P.; Toghraie, D.; Dehkordi, R. B.; Afrand, M. Mixed convection of non-Newtonian nanofluid in an H-shaped cavity with cooler and heater cylinders filled by a porous material: Two phase approach. *Adv. Powder Technol.* **2019**, *30*, 2666–2685.

(11) Moraveji, A.; Toghraie, D. Computational fluid dynamics simulation of heat transfer and fluid flow characteristics in a vortex tube by considering the various parameters. *Int. J. Heat Mass Transfer* **2017**, *113*, 432–443.

(12) Mashayekhi, R.; Khodabandeh, E.; Akbari, O. A.; Toghraie, D.; Bahiraei, M.; Gholami, M. CFD analysis of thermal and hydrodynamic characteristics of hybrid nanofluid in a new designed sinusoidal double-layered microchannel heat sink. *J. Therm. Anal. Calorim.* **2018**, *134*, 2305–2315.

(13) Abu-Hamdeh, N. H.; Alsulami, R. A.; Rawa, M. J.; Alazwari, M. A.; Goodarzi, M.; Safaei, M. R. A Significant Solar Energy Note on Powell-Eyring Nanofluid with Thermal Jump Conditions: Implementing Cattaneo-Christov Heat Flux Model. *Mathematics* **2021**, *9*, 2669.

(14) Alazwari, M. A.; Abu-Hamdeh, N. H.; Goodarzi, M. Entropy optimization of first-grade viscoelastic nanofluid flow over a stretching sheet by using classical Keller-box scheme. *Mathematics* **2021**, *9*, 2563.

(15) Alazwari, M. A.; Safaei, M. R. Non-isothermal hydrodynamic characteristics of a nanofluid in a fin-attached rotating tube bundle. *Mathematics* **2021**, *9*, 1153.

(16) Rozati, S. A.; Montazerifar, F.; Ali Akbari, O.; Hoseinzadeh, S.; Nikkhah, V.; Marzban, A.; Goodarzi, M. Natural convection heat transfer of water/Ag nanofluid inside an elliptical enclosure with different attack angles. *Math. Meth. Appl. Sci.* **2020**, DOI: 10.1002/mma.7036.

(17) Imran, M.; Farooq, U.; Waqas, H.; Anqi, A. E.; Safaei, M. R. Numerical performance of thermal conductivity in Bioconvection flow of cross nanofluid containing swimming microorganisms over a cylinder with melting phenomenon. *Case Studies in Thermal Engineering* **2021**, *26*, No. 101181.

(18) Li, Z. X.; Khaled, U.; Al-Rashed, A. A.; Goodarzi, M.; Sarafraz, M. M.; Meer, R. Heat transfer evaluation of a micro heat exchanger cooling with spherical carbon-acetone nanofluid. *Int. J. Heat Mass Transfer* **2020**, *149*, No. 119124.

(19) Kristiawan, B.; Wijayanta, A. T.; Enoki, K.; Miyazaki, T.; Aziz, M. Heat transfer enhancement of TiO<sub>2</sub>/water nanofluids flowing inside a square minichannel with a microfin structure: A numerical investigation. *Energies* **2019**, *12*, 3041.

(20) Kristiawan, B.; Rifa'i, A. I.; Enoki, K.; Wijayanta, A. T.; Miyazaki, T. Enhancing the thermal performance of TiO<sub>2</sub>/water nanofluids flowing in a helical microfin tube. *Powder Technol.* **2021**, *376*, 254–262.

(21) Purnama, B.; Rahmawati, R.; Wijayanta, A. T.; Suharyana, S. Dependence of structural and magnetic properties on annealing times in Co-precipitated cobalt ferrite nanoparticles. *J. Magn.* **2015**, *20*, 207–210.

(22) Purnama, B.; Arilasita, R.; Rikamukti, N.; Budiawanti, S.; Wijayanta, A. T.; Djuhana, D.; Matsuyama, K. Annealing temperature dependence of crystalline structure and magnetic properties in nano-powder strontium-substituted cobalt ferrite. *Nano-Struct. Nano-Objects* **2022**, *30*, No. 100862.

(23) Tahir, F.; Gul, T.; Islam, S.; Shah, Z.; Khan, A.; Khan, W.; Ali, L.; Muradullah. Flow of a nano-liquid film of Maxwell fluid with thermal radiation and magneto hydrodynamic properties on an unstable stretching sheet. *J. Nanofluids* **2017**, *6*, 1021–1030.

(24) Nadeem, S.; Haq, R. U.; Khan, Z. H. Numerical study of MHD boundary layer flow of a Maxwell fluid past a stretching sheet in the presence of nanoparticles. *J. Taiwan Inst. Chem. Eng.* **2014**, *45*, 121–126.

(25) Binetti, L.; Stankiewicz, A.; Alwis, L. Measurement of viscoelasticity of sodium alginate by fibre Bragg grating. In *Multidisciplinary Digital Publishing Institute Proceedings*, 2019; (Vol. 15, No. 1, pp. 1–33).

(26) Pawar, S. S.; Sunnapwar, V. K. Experimental studies on heat transfer to Newtonian and non-Newtonian fluids in helical coils with laminar and turbulent flow. *Exp. Therm. Fluid Sci.* **2013**, *44*, 792–804.

(27) Kumar, S.; Bhanjana, G.; Sharma, A.; Sidhu, M. C.; Dilbaghi, N. Synthesis, characterization and on field evaluation of pesticide loaded sodium alginate nanoparticles. *Carbohydr. Polym.* **2014**, *101*, 1061–1067.

(28) Mohammed Fayaz, A.; Balaji, K.; Girilal, M.; Kalaichelvan, P. T.; Venkatesan, R. Mycobased synthesis of silver nanoparticles and their incorporation into sodium alginate films for vegetable and fruit preservation. *J. Agric. Food Chem.* **2009**, *57*, 6246–6252.

(29) Bahiraei, M.; Godini, A.; Shahsavari, A. Thermal and hydraulic characteristics of a minichannel heat exchanger operated with a non-Newtonian hybrid nanofluid. *J. Taiwan Inst. Chem. Eng.* **2018**, *84*, 149–161.

(30) Al-Rashed, A. A.; Shahsavari, A.; Entezari, S.; Moghimi, M. A.; Adio, S. A.; Nguyen, T. K. Numerical investigation of non-Newtonian water-CMC/CuO nanofluid flow in an offset strip-fin microchannel heat sink: thermal performance and thermodynamic considerations. *Appl. Therm. Eng.* **2019**, *155*, 247–258.

(31) Naganthran, K.; Nazar, R.; Pop, I. Effects of heat generation/absorption in the Jeffrey fluid past a permeable stretching/shrinking disc. *J. Braz. Soc. Mech. Sci. Eng.* **2019**, *41*, 1–12.

(32) Hemmat, E. M. On the evaluation of the dynamic viscosity of non-Newtonian oil based nanofluids. *J. Therm. Anal. Calorim.* **2019**, *135*, 97–109.

(33) Naganthran, K.; Nazar, R.; Pop, I. Unsteady stagnation-point flow and heat transfer of a special third grade fluid past a permeable stretching/shrinking sheet. *Sci. Rep.* **2016**, *6*, 1–13.

(34) El-Zahar, E. R.; Rashad, A. M.; Saad, W.; Seddek, L. F. Magneto-hybrid nanofluids flow via mixed convection past a radiative circular cylinder. *Sci. Rep.* **2020**, *10*, 1–13.

(35) Rashad, A. M.; Chamkha, A. J.; Ismael, M. A.; Salah, T. Magneto-hydrodynamics natural convection in a triangular cavity filled with a Cu-Al<sub>2</sub>O<sub>3</sub>/water hybrid nanofluid with localized heating from below and internal heat generation. *J. Heat Transfer* **2018**, *140* (), DOI: 10.1115/1.4039213.

(36) Gorla, R. S. R.; Siddiqua, S.; Mansour, M. A.; Rashad, A. M.; Salah, T. Heat source/sink effects on a hybrid nanofluid-filled porous cavity. *J. Thermophys. Heat Transfer* **2017**, *31*, 847–857.

(37) Nayak, M. K.; Akbar, N. S.; Pandey, V. S.; Khan, Z. H.; Tripathi, D. 3D free convective MHD flow of nanofluid over permeable linear stretching sheet with thermal radiation. *Powder Technol.* **2017**, *315*, 205–215.

(38) Zainal, N. A.; Nazar, R.; Naganthran, K.; Pop, I. MHD flow and heat transfer of hybrid nanofluid over a permeable moving surface in the presence of thermal radiation. *Int. J. Numer. Methods Heat Fluid Flow* **2021**.

(39) Cess, R. D. The interaction of thermal radiation with free convection heat transfer. *Int. J. Heat Mass Transfer* **1966**, *9*, 1269–1277.

(40) Arpaci, V. S. Effect of thermal radiation on the laminar free convection from a heated vertical plate. *Int. J. Heat Mass Transfer* **1968**, *11*, 871–881.

(41) Agbaje, T. M.; Mondal, S.; Motsa, S. S.; Sibanda, P. A numerical study of unsteady non-Newtonian Powell-Eyring nanofluid flow over a shrinking sheet with heat generation and thermal radiation. *Alexandria Eng. J.* **2017**, *56*, 81–91.

(42) Gul, T.; Noman, W.; Sohail, M.; Khan, M. A. Impact of the Marangoni and thermal radiation convection on the graphene-oxide-water-based and ethylene-glycol-based nanofluids. *Adv. Mech. Eng.* **2019**, *11*, 1687814019856773.

(43) Gul, T. Scattering of a thin layer over a nonlinear radially extending surface with Magneto hydrodynamic and thermal dissipation. *Surf. Rev. Lett.* **2019**, *26*, 1850123.

(44) Bazdar, H.; Toghraie, D.; Pourfattah, F.; Akbari, O. A.; Nguyen, H. M.; Asadi, A. Numerical investigation of turbulent flow and heat transfer of nanofluid inside a wavy microchannel with different wavelengths. *J. Therm. Anal. Calorim.* **2020**, *139*, 2365–2380.

(45) Arasteh, H.; Mashayekhi, R.; Goodarzi, M.; Motaharpour, S. H.; Dahari, M.; Toghraie, D. Heat and fluid flow analysis of metal foam embedded in a double-layered sinusoidal heat sink under local thermal non-equilibrium condition using nanofluid. *J. Therm. Anal. Calorim.* **2019**, *138*, 1461–1476.

(46) Algarni, M.; Alazwari, M. A.; Safaei, M. R. Optimization of nano-additive characteristics to improve the efficiency of a shell and tube thermal energy storage system using a hybrid procedure: DOE, ANN, MCDM, MOO, and CFD modeling. *Mathematics* **2021**, *9*, 3235.

(47) Soudagar, M. E. M.; Khan, H. M.; Khan, T. Y.; Razaq, L.; Asif, T.; Mujtaba, M. A.; Safaei, M. R. Experimental analysis of engine performance and exhaust pollutant on a single-cylinder diesel engine operated using moringa oleifera biodiesel. *Appl. Sci.* **2021**, *11*, 7071.

(48) Wategave, S. P.; Banapurmath, N. R.; Sawant, M. S.; Soudagar, M. E. M.; Mujtaba, M. A.; Afzal, A.; Sajjan, A. M. Clean combustion and emissions strategy using reactivity controlled compression ignition (RCCI) mode engine powered with CNG-Karanja biodiesel. *J. Taiwan Inst. Chem. Eng.* **2021**, *124*, 116–131.

(49) Harari, P. A.; Banapurmath, N. R.; Yaliwal, V. S.; Soudagar, M. E. M.; Khan, T. Y.; Mujtaba, M. A.; EL-Seesy, A. I. Experimental investigation on compression ignition engine powered with pentanol and thevetia peruviana methyl ester under reactivity controlled compression ignition mode of operation. *Case Studies in Thermal Engineering* **2021**, *25*, No. 100921.

(50) Makarim, D. A.; Suami, A.; Wijayanta, A. T.; Kobayashi, N.; Itaya, Y. Marangoni convection within thermosolute and absorptive aqueous LiBr solution. *Int. J. Heat Mass Transfer* **2022**, *188*, No. 122621.

(51) Takabi, B.; Salehi, S. Augmentation of the heat transfer performance of a sinusoidal corrugated enclosure by employing hybrid nanofluid. *Adv. Mech. Eng.* **2014**, *6*, 147059.

(52) Qasim, M.; Khan, Z. H.; Lopez, R. J.; Khan, W. A. Heat and mass transfer in nanofluid thin film over an unsteady stretching sheet using Buongiorno's model. *Eur. Phys. J. Plus* **2016**, *131*, 1–11.

(53) Chahregh, H. S.; Dinarvand, S. TiO<sub>2</sub>-Ag/blood hybrid nanofluid flow through an artery with applications of drug delivery and blood circulation in the respiratory system. *Int. J. Numer. Methods Heat Fluid Flow* **2020**.

(54) Gul, T.; Pervez, R. Thin-film Maxwell hybrid nanofluid flow over an unsteady inclined stretching sheet in terms of nonlinear mixed convection. *Waves in Random and Complex Media* **2022**, 1–19.

(55) Zainal, N. A.; Nazar, R.; Naganthran, K.; Pop, I. Unsteady flow of a Maxwell hybrid nanofluid past a stretching/shrinking surface with thermal radiation effect. *Appl. Math. Mech.* **2021**, *42*, 1511–1524.

(56) Aziz, A.; Jamshed, W.; Ali, Y.; Shams, M. Heat transfer and entropy analysis of Maxwell hybrid nanofluid including effects of inclined magnetic field, Joule heating and thermal radiation. *Discrete & Continuous Dynamical Systems-S* **2020**, *13*, 2667.

(57) Almakki, M.; Nandy, S. K.; Mondal, S.; Sibanda, P.; Sibanda, D. A model for entropy generation in stagnation-point flow of non-Newtonian Jeffrey, Maxwell, and Oldroyd-B nanofluids. *Heat Trans. - Asian Res.* **2019**, *48*, 24–41.

(58) Gul, T.; Qadeer, A.; Alghamdi, W.; Saeed, A.; Mukhtar, S.; Jawad, M. Irreversibility analysis of the couple stress hybrid nanofluid flow under the effect of electromagnetic field. *Int. J. Numer. Methods Heat Fluid Flow* **2022**.

(59) Hayat, T.; Khan, S. A.; Alsaedi, A.; Fardoun, H. M. Heat transportation in electro-magneto-hydrodynamic flow of Darcy-Forchheimer viscous fluid with irreversibility analysis. *Phys. Scr.* **2020**, *95*, 105214.

(60) Kurnia, J. C.; Chaedir, B.; Wijayanta, A. T.; Sasmito, A. P. Convective Heat Transfer Enhancement of Laminar Herschel–Bulkley Non-Newtonian Fluid in Straight and Helical Heat Exchangers with Twisted Tape Inserts. *Ind. Eng. Chem. Res.* **2022**, *61*, 814–844.